JNS 2 (2012) 113-124

Journal of
NANOSTRUCTURES
JNS
NANOSTRUCTURES
JNS.kashanu.ac.ir

Electro-Thermo-Mechanical Response of Thick-Walled Piezoelectric Cylinder Reinforced by BNNTs

A. Ghorbanpour Arani[a,b,*], A. Haghshenas[c], S. Amir [a], M. Azami[a], Z. Khoddami Maraghi[a]

[a]*Faculty of Mechanical Engineering,* [b]*Institute of Nanoscience & Nanotechnology,University of Kashan, Kashan, I.R.Iran.*

[c]*Departement of Mechanical Engineering of Isalamic Azad University of Khomaynishahr, I.R.Iran.*

Article history:
Received 24/1/2012
Accepted 20/4/2012
Published online 1/6/2012

Keywords:
Boron Nitride Nanotube
Piezoelectric cylinder
Electro-thermo-mechanical-analysis
Micromechanical model

**Corresponding author:*
E-mail address*:*
aghorban@kashanu.ac.ir
Phone: +98 9131626594
Fax: +98 3615912424

Abstract

Electro-thermo-elastic stress analysis of piezoelectric polymeric thick-walled cylinder reinforced by boronnitride nanotubes (BNNTs) subjected to electro-thermo-mechanical fields is presented in this article. The electro-thermo-elastic properties of piezoelectric fiber reinforced composite (PEFRC) was studied by a modified XY micromechanical model capable of exhibiting full coupling relation between electric, thermal and elastic fields. Assuming the basic relation for the axisymmetric deformation of a thick-wall cylinder subjected to uniform internal and external pressures, an axial electrical load, a temperature change ΔT between inner and outer radius are derived. The stress results suggest that increasing BNNTs content in longitudinal direction reduces the effective stress. Also, displacement along radial direction indicates an optimum content of 5% BNNT for this. Furthermore, at normal working conditions, the influence of thermal and mechanical fields are much higher than the electric one on the effective stress; hence, this smart structure is best suited for applications as sensors than actuators.

1. Introduction

Electro-elastic materials are known to exhibit electromechanical coupling characteristics. They experience mechanical deformations when placed in an electric field, and become electrically polarized under mechanical loads [1]. Lately, smart composites, including piezoelectric composites under electro-thermo-mechanical fields, have been studied for extensive applications in power generation, sensors, actuators, ultrasonic transducer,aircraft and space platforms, automobile industries, offshore and submarine structures, chemical vessels and civil engineering structures [2-6]. These structures can be simplified to an

orthotropic hollow cylinder, and exposed to a variety of temperature fields in various environments. Understanding mechanical behavior of these composites is prerequisite in allocating their appropriate applications. Recently, nano sized tubes such as carbon nanotubes (CNTs) and BNNTshave been used as reinforcement in composite structures with the latter having higher thermal conductivity, better oxidation resistance at higher temperatures, and superior mechanical properties [7].

In 1969, Kawai [8] discovered a significant piezoelectric effect in polyvinylidene fluoride (PVDF) and considering its excellent mechanical properties while subjected to temperature continuously, PVDF has since been extensively studied [9, 10].Bent and Hagood[11] suggested first the use of piezoelectric composite actuators for structural applications. Concept and model of a piezoelectric structural fiber for multifunctional composites was investigated by Lin and Sodano[12]. A semi-analytical method for analyzing prismatic non-homogeneous piezoelectric cylinders with arbitrary cross-sectional geometry was presented by Liu and Taciroglu [13]. Using a general stress analysis, Sayman [14] developed a model for thick or thin multi-layered composite cylinders under hydrothermal loadings and solved it for plane-strain, open and closed ends cases. Wang and Zhong [15] derived an exact solution for a two-dimensional problem of an infinitely longcircular tube or bar of cylindrically anisotropic magneto-electro-elastic material under pressure load and applied the Stroh formalism for a cylindrical coordinate system. In another work, [16] investigated a finitely long laminated orthotropic circular cylindrical shell under pressure load and a uniform temperature change and applied power series together with Fourier series expansion methods.A three-phase cylindrical model was also used by Tong et al.[17]to analyze a fiber composite subjected to in-plane mechanical loads under the coupling effects of thermo, electric, magnetic and elastic fields. Frankland et al.[18]studied stress–strain curves of a polyethylene–single walled CNT (SWCNT) composite prepared by molecular dynamic simulations.Ding et al. [19] proposed an analytical method to solve the axisymmetric plane strain piezo-thermo-elastic dynamic problems of a special non-homogeneous pyroelectric hollow cylinder subjected to arbitrary axisymmetric thermal loads. Dai and Wang [20]presented an exact solution for thermo-electro-elastic transient response in piezoelectric hollowstructures subjected to arbitrary thermal, radial and electric shock loads.

In this work, the stress analysis of a piezoelectric polymeric thick-walled cylinder(e.g. PVDF) reinforced by another piezoelectric material such as BNNTs and subjected to electro-thermo-elastic loading is studied. Overall properties of the piezoelectric fiber reinforced composite (PEFRC) material are evaluated as suggested by Tan & Tong [21] using an XY micro-mechanic model. Employing equilibrium equations in the cylindrical coordinate for a thick-walled cylinder, and overall properties applied in the stress-strain-temperature-electric field relation, a differential equation for radial displacement is derived, which is then solved in exact form for the specified boundary conditions. Replacing the obtained radial displacement in the stress-strain relation yields radial, longitudinal and circumferential stresses, which are plotted for various boundary conditions, against temperature difference, potential difference and cylinder radius.

2. Micro-mechanic model

As mentioned above the overall properties of the PEFRC is evaluated by a micro-mechanic XY model. A representative volume element (RVE) with square cross-sectional is selected for a PEFRC and a circular one for the fiber is assumed (see Fig.1). The influence of the piezoelectric fiber volume fraction on the effective constants for PEFRC materials using the above mentioned model was investigated and the results complied well with those found with Mori-Tanaka mean field approach. The assumptions made for the XY model include:

The composite material is perfectly bonded, its constituents are assumed to be linear homogeneous and orthotropic.

The applied electric and thermal fields to the PEFRC unit cell are uniform.

Iso-stress, iso-electric displacement, are assumed to exist across the planes which are in series with respect to the loading direction. Iso-strain and iso-electric field are assumed across the planes which are in parallel with respect to the loading direction [6].

Thermal field within a PEFRC unit cell is uniform.

The closed-form formulas for the effective electro-thermo-elastic constants of an X PEFRC strip may be expressed as equations 1.1 to 1.11 described below

$$C^{p}_{11} = \frac{C^{mm}_{11}\ C^{pp}_{11}}{\rho C^{mm}_{11} + (1-\rho)C^{pp}_{11}}, \tag{1.1}$$

$$C^{p}_{22} = \rho C^{pp}_{22} + (1-\rho)C^{mm}_{22} + \frac{(C^{p}_{12})^2}{(C^{p}_{11})} - \rho\frac{(C^{pp}_{12})^2}{C^{pp}_{11}} - \frac{(1-\rho)(C^{mm}_{12})^2}{C^{mm}_{11}}, \tag{1.2}$$

$$C^{p}_{23} = \rho C^{pp}_{23} + (1-\rho)C^{mm}_{23} + \frac{C^{p}_{12}C^{p}_{13}}{C^{p}_{11}} - \rho\frac{C^{pp}_{12}C^{pp}_{13}}{C^{pp}_{11}} - \frac{(1-\rho)C^{mm}_{12}C^{mm}_{13}}{C^{mm}_{11}}, \tag{1.3}$$

$$C^{p}_{13} = C^{p}_{11}\left[\frac{\rho C^{pp}_{13}}{C^{pp}_{11}} - \frac{(1-\rho)C^{mm}_{13}}{C^{mm}_{11}}\right], \tag{1.4}$$

$$C^{p}{}_{33} = \rho C^{pp}_{33} + (1-\rho)C^{mm}_{33} + \frac{(C^{p}_{13})^2}{C^{p}{}_{12}} - \rho\frac{(C^{pp}_{3})^2}{C^{pp}_{11}} - \frac{(1-\rho)(C^{mm}_{13})^2}{C^{mm}_{11}}, \tag{1.5}$$

$$e^{p}{}_{31} = C^{p}_{11}\left[\frac{\rho e^{pp}_{13}}{C^{pp}_{11}} - \frac{(1-\rho)e^{mm}_{13}}{C^{mm}_{11}}\right], \tag{1.6}$$

$$e^{p}{}_{32} = \rho e^{pp}_{23} + (1-\rho)e^{mm}_{23} + \frac{C^{p}_{12}e^{p}_{13}}{C^{p}_{11}} - \rho\frac{C^{pp}_{12}e^{pp}_{13}}{C^{pp}_{11}} - \frac{(1-\rho)C^{mm}_{12}e^{mm}_{13}}{C^{mm}_{11}}, \tag{1.7}$$

$$e^{p}{}_{33} = \rho e^{pp}_{33} + (1-\rho)e^{mm}_{33} + \frac{C^{p}_{13}e^{p}_{13}}{C^{p}_{11}} - \rho\frac{C^{pp}_{13}e^{pp}_{13}}{C^{pp}_{11}} - \frac{(1-\rho)C^{mm}_{13}e^{mm}_{13}}{C^{mm}_{11}}, \tag{1.8}$$

$$\lambda^{p}_{1} = C^{p}_{11}\left[\frac{\rho\lambda^{pp}_{1}}{C^{pp}_{11}} - \frac{(1-\rho)\lambda^{mm}_{11}}{C^{mm}_{11}}\right], \tag{1.9}$$

$$\lambda^{p}_{3} = \rho\lambda^{pp}_{3} + (1-\rho)\lambda^{mm}_{3} + \frac{C^{p}_{13}\lambda^{p}_{1}}{C^{p}_{11}} - \rho\frac{C^{pp}_{13}\lambda^{p}_{2}}{C^{pp}_{11}} - \frac{(1-\rho)C^{mm}_{13}\lambda^{mm}_{1}}{C^{mm}_{11}}, \tag{1.10}$$

$$\lambda^{p}_{2} = \rho\lambda^{pp}_{22} + (1-\rho)\lambda^{mm}_{22} + \frac{C^{p}_{12}\lambda^{p}_{1}}{C^{p}_{11}} - \rho\frac{C^{pp}_{12}\lambda^{p}_{2}}{C^{pp}_{11}} - \frac{(1-\rho)C^{mm}_{12}\lambda^{mm}_{1}}{C^{mm}_{11}}. \tag{1.11}$$

where C_{ij}, e_{mn} and λ_p, are elastic stiffness constants, piezoelectric constants and thermal expansion, respectively. The constant ρ is $x_a / x_b = y_a / y_b$ where x_a, x_b and y_a, y_b are dimensions of fiber and matrix unit cells, respectively, as illustrated in Fig. 1. For the Y PEFRC model, the corresponding equations can be obtained by simply exchanging the subscripts 1 with 2 in the above Eqs. (1.1-1.10). Hence, the effective constants of XY model was obtained by placing the effective constitutive coefficients of X model into the effective fiber coefficients of Y model. The resulting formulations are presented in Eqs. (1.12- 1.23) below which represent the mechanical properties for the defined RVE:

$$C_{11} = \rho C_{11}^{p} + (1-\rho)C_{11}^{m} + \frac{C_{12}^{2}}{C_{22}} - \rho\frac{(C_{12}^{p})^{2}}{C_{22}^{p}} - \frac{(1-\rho)(C_{12}^{m})^{2}}{C_{22}^{m}}, \tag{1.12}$$

$$C_{12} = C_{22}\left[\frac{\rho C_{12}^{p}}{C_{22}^{p}} - \frac{(1-\rho)C_{12}^{m}}{C_{22}^{m}}\right], \tag{1.13}$$

$$C_{13} = \rho C_{13}^{p} + (1-\rho)C_{13}^{m} + \frac{C_{12}C_{23}}{C_{22}} - \rho\frac{C_{12}^{p}C_{23}^{p}}{C_{22}^{p}} - \frac{(1-\rho)C_{12}^{m}C_{23}^{m}}{C_{22}^{m}}, \tag{1.14}$$

$$C_{22} = \frac{C_{22}^{p}C_{22}^{m}}{\rho C_{22}^{m} + (1-\rho)C_{22}^{p}}, \tag{1.15}$$

$$C_{23} = C_{22}\left[\frac{\rho C_{23}^{2}}{C_{22}^{p}} - \frac{(1-\rho)C_{23}^{m}}{C_{22}^{m}}\right], \tag{1.16}$$

$$C_{33} = \rho C_{33}^{p} + (1-\rho)C_{33}^{m} + \frac{C_{23}^{2}}{C_{22}} - \rho\frac{(C_{23}^{p})^{2}}{C_{22}^{p}} - \frac{(1-\rho)(C_{23}^{m})^{2}}{C_{22}^{m}}, \tag{1.17}$$

$$e_{31} = \rho e_{31}^{p} + (1-\rho)e_{31}^{m} + \frac{C_{12}e_{32}}{C_{22}} - \rho\frac{C_{12}^{p}e_{32}^{p}}{C_{22}^{p}} - \frac{(1-\rho)C_{12}^{m}e_{32}^{m}}{C_{22}^{m}}, \tag{1.18}$$

$$e_{32} = C_{22}\left[\frac{\rho e_{32}^{2}}{C_{22}^{p}} - \frac{(1-\rho)e_{32}^{m}}{C_{22}^{m}}\right], \tag{1.19}$$

$$e_{33} = \rho e_{33}^{p} + (1-\rho)e_{33}^{m} + \frac{C_{23}e_{32}}{C_{22}} - \rho\frac{C_{23}^{p}e_{32}^{p}}{C_{22}^{p}} - \frac{(1-\rho)C_{23}^{m}e_{32}^{m}}{C_{22}^{m}}, \tag{1.20}$$

$$\lambda_1 = \rho\lambda_1^{p} + (1-\rho)\lambda_1^{m} + \frac{C_{12}\lambda_2}{C_{22}} - \rho\frac{C_{12}^{p}\lambda_2^{p}}{C_{22}^{p}} - \frac{(1-\rho)C_{12}^{m}\lambda_2^{m}}{C_{22}^{m}}, \tag{1.21}$$

$$\lambda_3 = \rho\lambda_3^{p} + (1-\rho)\lambda_3^{m} + \frac{C_{23}\lambda_2}{C_{22}} - \rho\frac{C_{23}^{p}\lambda_2^{p}}{C_{22}^{p}} - \frac{(1-\rho)C_{23}^{m}\lambda_2^{m}}{C_{22}^{m}}, \tag{1.22}$$

$$\lambda_2 = C_{22}\left[\frac{\rho\lambda_2^{p}}{C_{22}^{p}} - \frac{(1-\rho)\lambda_2^{m}}{C_{22}^{m}}\right]. \tag{1.23}$$

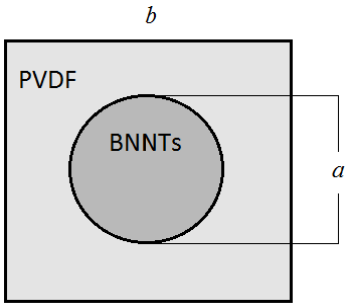

Fig. 1. Schematics of representative volume element.

3. Fundamental relations

Fig. 2 demonstrates a thick-walled cylinder, subjected to uniform internal and external pressures (P_i and P_o, respectively), and a radial temperature change ΔT, in an axial electrical field. The temperature change ΔT is a function of the radial coordinate r only and hence, cylinder deformation is axially symmetric. Furthermore, the deformations happen at a cross section sufficiently far removed from the junction of the cylinder and its end caps, so that it is practically independent of the axial coordinate z as suggested by Boresi et al. [22].

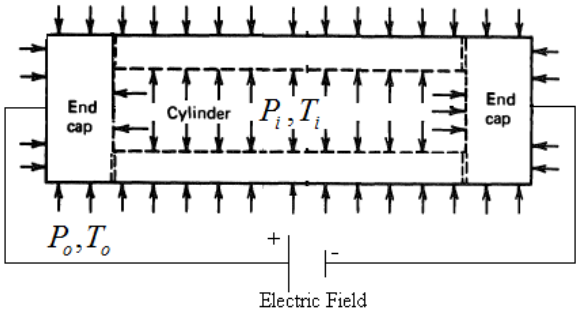

Fig. 2. A closed cylinder with internal pressure, external pressure, radial temperature and axial electric fields.

3.1. Heat Conduction Analysis

Steady-state temperature distribution in a homogeneous body in the absence of any heat source may be presented by the Fourier's heat equation as

$$\nabla^2 T = 0 \tag{2}$$

For symmetric thermal conduction, the heat equation in a cylindrical coordinate (r, θ, z) can be written as

$$\frac{\partial^2 T}{\partial r^2} + \frac{1}{r}\frac{\partial T}{\partial r} = 0 \tag{3}$$

which could be solved in the following form

$$T_r = k_1 + k_2 \ln(r) \tag{4}$$

where k_1 , k_2 are integration constants. The boundary conditions $T = T_i$ when $r = r_i$, and $T = T_o$ when $r = r_o$ allows k_1 and k_2 to be determined as

$$k_2 = \frac{(T_i - T_o)}{\ln(r_i) - \ln(r_o)}$$
$$k_1 = T_i - k_2 \, Ln(r_i) \tag{5}$$

3.2. Governing Equations

In thick-walled cylinder with end caps there are only three stress components of σ_r , σ_θ and σ_z (radial, circumferential and axial stresses, respectively) all of which are function of radius. Ignoring body force component, the equilibrium equation in radial direction becomes [22]

$$\frac{\partial \sigma_r}{\partial_r} + \frac{\sigma_r - \sigma_\theta}{r} = 0 \tag{6}$$

The electrical equilibrium equation is however [1]

$$\frac{1}{r}(rD_r)_{,r} + \frac{1}{r}D_{\theta,\theta} + D_{z,z} = 0 \tag{7}$$

where D_r , D_θ and D_z are component of radial, circumferential and longitudinal electric displacement, respectively.

The composite material of the cylinder is assumed to be orthotropic and linearly elastic. Therefore, the stress-strain-temperature-electric field relations may be given as [1]

$$\begin{bmatrix} \sigma_r \\ \sigma_\theta \\ \sigma_z \end{bmatrix} = \begin{bmatrix} C_{11} & C_{12} & C_{13} \\ C_{12} & C_{22} & C_{23} \\ C_{31} & C_{32} & C_{33} \end{bmatrix} \begin{bmatrix} \varepsilon_r \\ \varepsilon_\theta \\ \varepsilon_z \end{bmatrix} - \begin{bmatrix} 0 & 0 & e_{13} \\ 0 & 0 & e_{23} \\ 0 & 0 & e_{33} \end{bmatrix} \begin{bmatrix} E_r \\ E_\theta \\ E_z \end{bmatrix} - \begin{bmatrix} \lambda_r \\ \lambda_\theta \\ \lambda_z \end{bmatrix} \Delta T, \tag{8}$$

and

$$\begin{bmatrix} D_r \\ D_\theta \\ D_z \end{bmatrix} = \begin{bmatrix} 0 & 0 & 0 \\ 0 & 0 & 0 \\ e_{31} & e_{32} & e_{33} \end{bmatrix} \begin{bmatrix} \varepsilon_r \\ \varepsilon_\theta \\ \varepsilon_z \end{bmatrix} + \begin{bmatrix} \in_{11} & 0 & 0 \\ 0 & \in_{22} & 0 \\ 0 & 0 & \in_{33} \end{bmatrix} \begin{bmatrix} E_r \\ E_\theta \\ E_z \end{bmatrix}, \tag{9}$$

where λ_r, λ_θ , λ_z may also be expressed as

$$\begin{aligned} \lambda_r &= C_{11}\alpha_r + C_{12}\alpha_\theta + C_{13}\alpha_z \\ \lambda_\theta &= C_{21}\alpha_r + C_{22}\alpha_\theta + C_{23}\alpha_z \\ \lambda_z &= C_{31}\alpha_r + C_{32}\alpha_\theta + C_{33}\alpha_z . \end{aligned} \tag{10}$$

where ε and α correspond to strain and thermal expansion, respectively, and subscript r, θ and z denote respectively the radial, circumferential and longitudinal components. The strain-displacement relations are therefore

$$\varepsilon_r = \frac{\partial u_r}{\partial r}$$

$$\varepsilon_\theta = \frac{u_r}{r}, \tag{11}$$

$$\varepsilon_z = \frac{\partial u_z}{\partial z} .$$

where $u_r = u_r(r,z)$ and $u_z = u_z(r,z)$ represents displacement components in the r and z direction, respectively [21]. It should be noted that $\in_{33}$ and E_z represent dielectric constant and electric field in longitudinal direction, respectively and

$$E_z = -\frac{\partial \phi}{\partial z} . \tag{12}$$

Since u_r and u_z do not depend much on z at a cross section far removed from the end, the shear strain components become zero due to radial symmetry, in which case ε_z could be assumed constant, therefore

$$\varepsilon_z = \frac{\partial u_z}{\partial z} = a. \tag{13}$$

4. AnalyticalSolution

In order to solve this problem, the exact solution is adopted. The electric field is applied in z direction. However, considering Eq. (9), D_r and D_θ are zero, therefore Eq. (7) reduces to

$$\frac{\partial D_z}{\partial z} = 0 \tag{14}$$

Considering D_z component in Eq.(9), and Eq.(13), the electrical equilibrium Eq.(14) may be written as the following differential equation

$$\in_{33} \frac{\partial^2 \phi_z}{\partial z^2} = 0 \tag{15}$$

which could be solved by multiple integration with respect to z into the following format

$$\phi_z = \alpha z + \beta \tag{16}$$

where α and β are integral constants to be evaluated considering the two boundary conditions below on a thick-walled piezoelectric cylinder

$$\begin{aligned} &\phi_z = \phi_0; \qquad at \;\; z = 0 \\ &\phi_z = \phi_L; \qquad at \;\; z = L \end{aligned} \tag{17}$$

which yield

$$\begin{aligned} \beta &= \phi_0 \\ \alpha &= \frac{\phi_L - \phi_0}{L} \end{aligned} \tag{18}$$

.

The governing differential equation for the problem can now be obtained by substituting Eqs. (8), (10), (11), (13) and (16), into Eq. (6)

$$\begin{aligned} &C_{11} \times r^2 \times \frac{\partial^2 u_r}{\partial z^2} + C_{11} \times r \times (\frac{\partial u_r}{\partial r}) - C_{22}(u_r) = \\ &P \times r + Q \times r \times \ln r + r \times a \times k, \end{aligned} \tag{19}$$

where Q , P , k , N , M are constants, defined as

$$\begin{aligned} k &= (C_{23} - C_{13}) \\ M &= (\lambda_r - \lambda_\theta) \\ N &= (e_{32} - e_{31}) \end{aligned} \tag{20}$$

$$P = (N + Mk_1 + \lambda_r \times k_2)$$
$$Q = (Mk_2)$$

The governing Eq. (19) is the Cauchy-Euler non-homogeneous differential equation whose solution is

$$u_r = C_1 r^{A_1} + C_2 r^{-A_1} + A_2 \times r \times \ln r + A_3 \times r + A_4 \times a \times r, \quad (21)$$

where C_1 and C_2 are constants which could be obtained from boundary condition associated with internal and external pressure stresses explained below. A_1, A_2, A_3 and A_4 are constants defined as

$$A_1 = \left(\frac{C_{22}}{C_{11}}\right)^{0.5}$$
$$A_2 = \frac{Q}{C_{11} - C_{22}}$$
$$A_3 = \frac{C_{11}(P - 2Q) - C_{22}P}{(C_{11} - C_{22})^2} \quad (22)$$
$$A_4 = \frac{k}{C_{11} - C_{22}}$$

Substituting Eq. (21) into Eq. (11) and substituting the resulting equation into the first row of Eq. (8), yields the expression for radial stress (σ_r) as

$$\sigma_r = C_1 r^{H_1} \times H_2 + C_2 r^{H_3} \times H_4 + G_1 \ln r + G_2 + G_3 \times a \quad (23)$$

where the following constants could be defined as

$$H_1 = A_1 - 1$$
$$H_2 = (C_{11} A_1 + C_{12})$$
$$H_3 = (-A_1 - 1) \quad (24)$$
$$H_4 = [C_{11}(-A_1) + C_{12}]$$
$$G_1 = (C_{11} \times A_2 + C_{12} \times A_2 - \lambda_r \times k_2)$$
$$G_2 = (A_2 \times C_{11} + A_3 \times C_{11} + C_{12} \times A_3 + e_{13} \times \alpha - \lambda_r \times k_1)$$
$$G_3 = (A_4 \times C_{11} + C_{12} \times A_4 + C_{13})$$

In order to find C_1 and C_2 in Eq. (23) above, the following pressure boundary conditions on the inner and outer surfaces of the cylinder are considered

$$\sigma_r = -P_i; \quad at \quad r = r_i$$
$$\sigma_r = -P_0; \quad at \quad r = r_0 \quad (25)$$

Replacing these in the radial stress Eq. (23) gives

$$C_1 = J_1 + J_2 \times a$$
$$C_2 = J_3 + J_4 \times a \quad (26)$$

where

$$J_1 = \left(r_i^{H_3} \times P_0 + r_i^{H_3} \times G_1 \times \ln(r_0) + r_i^{H_3} \times G_2 - P_i \times r_0^{H_3} - G_1 \times \ln(r_i) \times r_0^{H_3} - G_2 \times r_0^{H_3}\right) / \left(H_2(-r_i^{H_3} \times r_0^{H_1} + -r_0^{H_3} \times r_i^{H_1})\right)$$
$$J_2 = \frac{r_i^{H_3} \times G_3 - G_3 \times r_i^{H_3}}{H_2(-r_i^{H_3} \times r_0^{H_1} + -r_0^{H_3} \times r_i^{H_1})}$$
$$J_3 = -\left(-r_0^{H_3} \times P_i + r_0^{H_1} \times G_1 \times \ln(r_i) + r_0^{H_1} \times G_2 - P_0 \times r_i^{H_1} + G_1 \times \ln(r_0) \times r_i^{H_1} - G_2 \times r_i^{H_1}\right) / \left(H_4(-r_i^{H_3} \times r_0^{H_1} + -r_0^{H_3} \times r_i^{H_1})\right) \quad (27)$$
$$J_4 = \frac{r_0^{H_1} \times G_3 - G_3 \times r_0^{H_1}}{H_4(-r_i^{H_3} \times r_0^{H_1} + -r_0^{H_3} \times r_i^{H_1})}$$

As can be seen C_1 and C_2 are defined in term of another constant a which need be determined considering another boundary condition, i.e. the equation for overall equilibrium forces along the longitudinal axial direction. This equation is obtained by balancing the axial electrical and mechanical forces involved and may be written as

$$\int_{r_i}^{r_0} \sigma_z \times 2\pi \times r \times dr = e_{33} \times (\alpha) \times \pi \times (r_0^2 - r_i^2) + \pi \times (P_i r_i^2 - P_0 r_0^2) \quad (28)$$

It is worth noting that the temperature change ΔT does not appear in Eq. (28). This is because the effects of temperature are self-equilibrating i.e. the thermal loads on the cylinder surface in longitudinal direction balances out each other and the overall thermal load becomes zero. Also, the electric field is considered as an axial load here that is applied to the cylinder closed ends. Eq. (28) may be one of the major contributions of this study, as it is perhaps the first time electric field is considered in this developed and solved governing equation in the form of an applied axial load for a three dimensional geometry. Other contributions of this paper include using the XY micromechanical model to evaluate the overall physical characteristics of the composite, which enabled us to compute both the overall piezoelectric and thermal constants of the composite on top of other mechanical properties associated with the problem. Assuming orthotropic matrix meant we had to choose the more complex XY model to solve the problem.

5. Numerical Results and discussion

At this point, numerical results are obtained for circumferential, longitudinal and effective stresses in a thick-walled composite cylinder made from PVDF and reinforced by DWBNNTs subjected to internal and external pressures, axial electric field and radial thermal field. Table 1 presents physical characteristics of both the orthotropic PVDF matrix and DWBNNTs reinforcement fibers of the smart composite used in this study [7] and [23].

The cylinder considered for this study is assumed to have inner radius 20×10^{-6} m, outer radius 23×10^{-6} m , length 100×10^{-6} m. Internal and external temperatures are 30ºC and 60ºC, respectively. Applied voltage is $\phi_0 = 1\times10^4$ volt. Internal and external pressures are assumed to be $-100\times10^6\, pa$ and zero, respectively. All quantities of stresses, displacements, temperatures and voltages have become dimensionless with respect to PVDF yield stress, σ_y, (σ_y=54 GPa), outer radius (r_o), internal temperature (T_i), and $\phi_L = 1\times10^4$ volt, respectively, as indicated in Eq. (29) below

$$\Sigma_r = \frac{\sigma_r}{\sigma_y}, \quad \Sigma_\theta = \frac{\sigma_\theta}{\sigma_y}, \quad \Sigma_z = \frac{\sigma_z}{\sigma_y},$$
$$\Sigma_e = \frac{\sigma_e}{\sigma_y}, \quad U_r = \frac{u_r}{r_o}, \quad R = \frac{r}{r_o}. \tag{29}$$

Table 1. Physical characteristics

Properties	BNNTs	PVDF
C_{11}	2.77 Tpa	10.64 Gpa
C_{12}	1.427 Tpa	1.92 Gpa
C_{13}	1.427 Tpa	2.19 Gpa
C_{22}	2.77 Tpa	23.6 Gpa
C_{23}	1.427 Tpa	3.98 Gpa
C_{33}	2.77 Tpa	238.24 Gpa
e_{33}	0	-0.13
e_{23}	0	-0.145
e_{13}	0.95	-0.276
α_r	0.6×10-6	7.1×10-5
α_θ	0.6×10-6	7.1×10-5
α_z	1.2×10-6	7.1×10-5

Fig. 3 shows the graph of dimensionless radial displacement, Ur, against cylinder radius, R, for various DWBNNT contents (ρ). Addition of DWBNNT increases cylinder stiffness considerably and reduces the radial displacement. The slope in this diagram indicates that the cylinder radial strain (ε_r), is maximum at $\rho = 0\%$, and almost zero for all other ρ's. This is expected as small addition of DWBNNTs has reduced

considerably ε_r. The improvement in reduction of radial displacement due to incremental addition of ρ is more significant with the smallest increase taking place at $\rho = 5\%$, leading to largest drop in radial displacement indicating that possibly 5% is the optimum DWBNNT content for the cylinder investigated here.

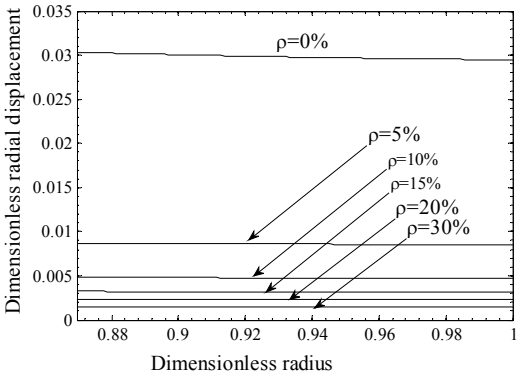

Fig. 3. Dimensionless radial displacement versus the radius of the smart composite cylinder for different content of DWBNNT.

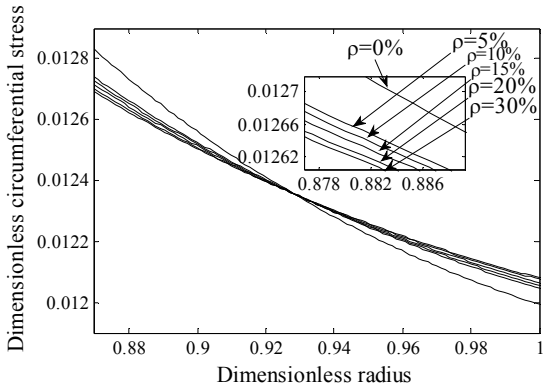

Fig. 4. Dimensionless circumferential stress versus the radius of the smart composite cylinder for different content of DWBNNT.

Figs. 4, 5 and 6 illustrate the dimensionless circumferential stress, axial stress and effective stress against the cylinder radius for different ρ's. As can be seen, the maximum circumferential stress occurs at the internal radius of the cylinder (0.87), and the maximum axial stress occurs at the external radius. Effective stress obtained on the basis of von Mises indicates that it is maximum at both internal and external radii of the cylinder. As ρ is increased from 0 to 30%, the maximum circumferential, axial and effective stresses are reduced to the extent that the effective stress is reduced by almost 75%. The same as Fig. 3, the significant incremental improvement in reduced circumferential stress, occurs at $\rho = 5\%$, indicating this value to be a possible optimum for crack resistance. It is also interesting to note that axial stress, σ_z, has become a function of the radius simply due to temperature difference across the internal and external radii, otherwise σ_z would have been a fixed value.

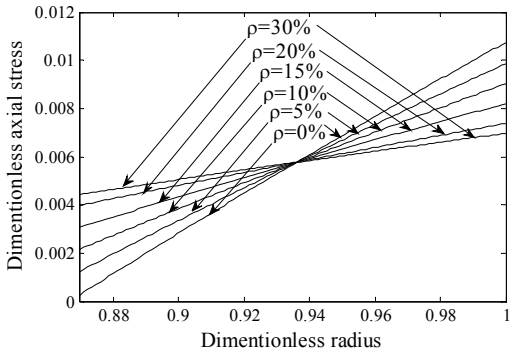

Fig. 5. Dimensionless axial stress versus the radius of the smart composite cylinder for different content of DWBNNT.

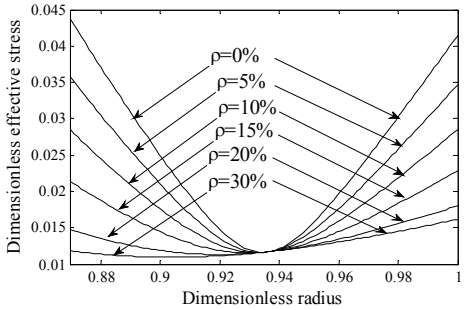

Fig. 6. Dimensionless effective stress (based on von Mises criterion) versus the radius of the smart composite cylinder for different content of DWBNNT.

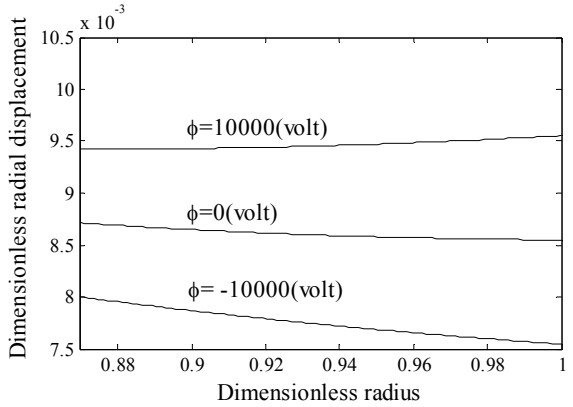

Fig. 7. Dimensionless radial displacement versus the radius of the smart composite cylinder for different voltages.

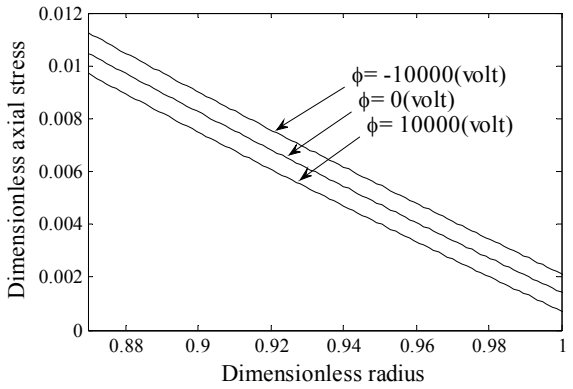

Fig. 8. Dimensionless circumferential stress versus the radius of the smart composite cylinder for different voltages.

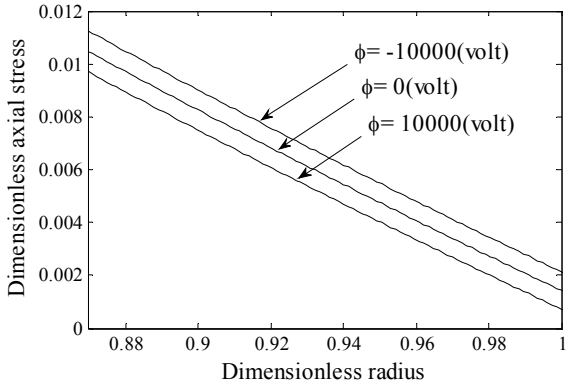

Fig. 9. Dimensionless axial stress versus the radius of the smart composite cylinder for different voltages.

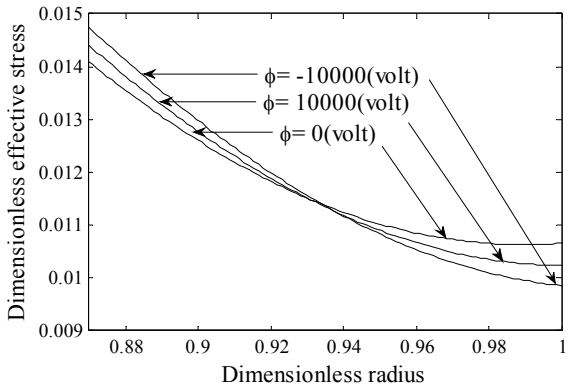

Fig. 10. Dimensionless effective stress versus the radius of the smart composite cylinder for different voltages.

Figs. 7, 8, 9 and 10 illustrate the effect of electric field on the Ur, Σ_θ, Σ_z and Σ_e along the radius of the cylinder at $\rho = 5\%$ and voltages of -10,000, 0 and +10,000 volt. As can be seen, the effect of electric field in general is insignificant. Nevertheless, it has caused more displacement at the outer radius of the cylinder and positive/negative voltages have led to positive/negative displacements, respectively. Maximum stresses occur at the internal radius of the cylinder at –negative voltage.

Considering the importance of temperature effects on the polymeric composite, Fig. 11 demonstrates the graphs of dimensionless radial displacement, U_r, versus r for three different internal temperatures, 30ºC, 45ºC and 60ºC, while the external temperature remains 30ºC. Maximum displacement occurs at the internal radius of the cylinder and increasing temperature causes increase in Ur.

Figs. 12, 13 and 14 illustrates the variations of Σ_θ, Σ_z and Σ_e along r for various internal temperatures of Ti =30ºC, 45ºC and 60ºC, while the external temperature To is kept constant at 30ºC. Maximum Σ_θ occurs at 30ºC at the internal radius of the cylinder and increase in the Ti leads to Σ_θ reduction. As can be seen in Fig. 13, in the

absence of temperature gradient between the inner and outer radii of the cylinder, (i.e. Ti = To =30ºC), the Σ_z is independent of R. Increase in Ti however, reduces Σ_z to a minimum at inner radius and increases Σ_z to a maximum at outer radius of the cylinder, which is justify able due to the self equilibrating nature of temperature field. This behaviour of the Σ_z however, indicate validation of the governing equations developed including Eq.(28). The effective stress (Fig. 14) at various Ti illustrate that Σ_e is maximum in the internal radius and is highest as Ti increases at both inner and outer radii of the smart composite cylinder.

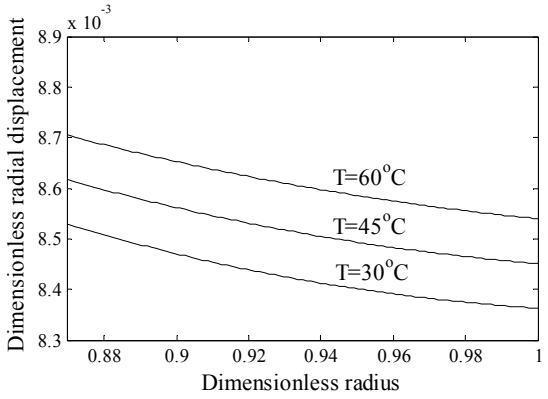

Fig. 11. Dimensionless radial displacement versus the radius of the smart composite cylinder for different internal temperatures, with external temperature at 30ºC.

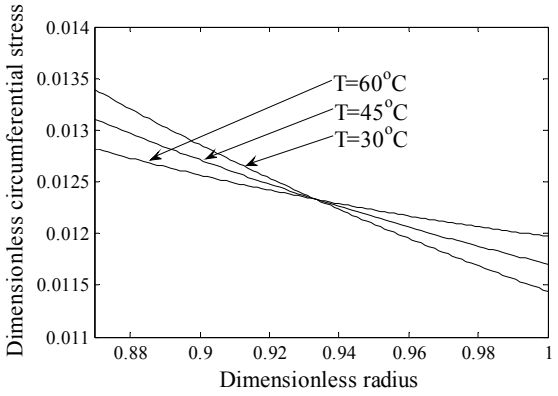

Fig. 12. Dimensionless circumferential stress versus the radius of the smart composite cylinder for different internal temperatures, with external temperature at 30ºC.

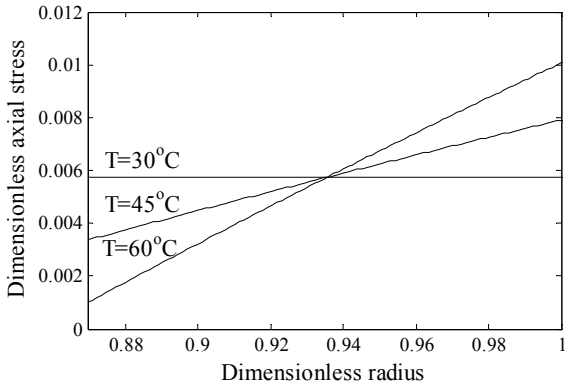

Fig. 13. Dimensionless axial stress versus the radius of the smart composite cylinder for different internal temperatures, with external temperature at 30ºC.

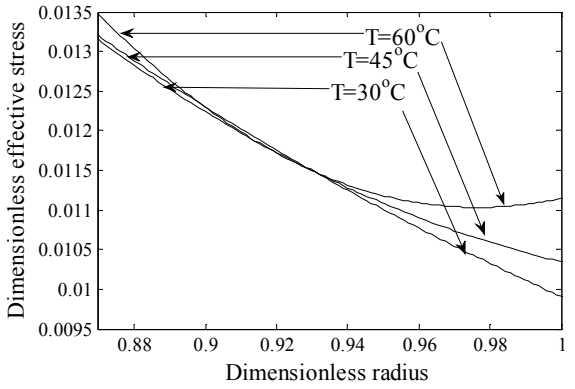

Fig. 14. Dimensionless effective stress versus the radius of the smart composite cylinder for different internal temperatures, with external temperature at 30ºC.

6. Conclusion

In this article, displacement, and circumferential, axial and effective stresses of a thick-walled smart composite cylinder with end-caps, made from piezoelectric materials (PVDF reinforced by DWBNNT's) and subjected to mechanical, electrical and thermal fields are studied. Apart from the piezoelectric nature of the materials used and the associated model for evaluating the overall mechanical characteristics, the contribution of the paper include consideration of 3-dimensional structural analysis and orthotropic composite

matrix. The results suggest that increasing DWBNNTs content reduces stresses associated with mechanical, thermal and electrical fields, in descending order. Also, at normal working conditions, the influence of thermal and mechanical fields are much higher than the electric one on the effective stress; hence, this smart structure is best suited for applications as sensors than actuators.

Acknowledgments

The authors are grateful to University of Kashan for sup porting this work by Grant No. 65475/11. They would also like to thank the Iranian Nanotechnology Development Committee for their financial support.

References

[1] J. Yang, An introduction to the theory of piezoelectricity, Springer, 2005.
[2] E.F. Crawley, AIAA J. 32 (1994) 1689.
[3] M. Arafa, A. Baz, Composites Part B. 31 (2000) 255.
[4] G. Park, M.H. Kim, D.J. Inman, J. Intell. Mater. Syst. Struct. 12 (2001) 423.
[5] H.A. Sodano, J. Lloyd, D.J. Inman, Smart Mater. Struct. 15 (2006) 1211.
[6] Y. Shindo, F. Narita, H. Sosa, Int. J. Eng. Sci. 38 (1998) 19.
[7] A. Salehi-Khojin, N. Jalili, Compos. Sci. Technol. 68 (2008) 489.
[8] H. Kawai, Jpn. J. Appl. Phys. 8 (1969) 975.
[9] W.V. Munch, U. Thiemann, Sens. Actuators A. 25 (1991) 167.
[10] H.S. Tzou, R. Ye, Mech. Syst. Sig. Process. 10 (1996) 459.
[11] A.A. Bent, N.W. Hagood, J. Intell. Mater. Syst. Struct. 8 (1997) 903.
[12] Y. Lin, H.A. Sodano, Compos. Sci. Technol. 68 (2008) 1911.
[13] C.W. Liu, E. Taciroglu, Int. J. Solids Struct. 45 (2008) 2379.
[14] O. Sayman, Composites Part A. 36 (2005) 923.
[15] X. Wang, Z. Zhong, Int. J. Eng. Sci. 41 (2003) 2143.
[16] X. Wang, Z. Zhong, Int. J. Eng. Sci. 41 (2003) 2429.
[17] Z.H. Tong, S.H. Lo, C.P. Jiang, Y.K. Cheung, Int. J. Solids Struct. 45 (2008) 5205.